




Commensurate and incommensurate magnetic structure of the moderately frustrated antiferromagnet $\text{Li}_2M(\text{WO}_4)_2$ with $M = \text{Co}, \text{Ni}$

Sunil K. Karna ^{1,*}, C. W. Wang ^{2,†}, R. Sankar,³ D. Temple ¹ and M. Avdeev^{4,5}

¹*Quantum Electronics Group, Department of Physics and Center for Materials Research, Norfolk State University, Norfolk, Virginia 23504, USA*

²*Neutron Group, National Synchrotron Radiation Research Center, Hsinchu 30076, Taiwan*

³*Institute of Physics, Academia Sinica, Taipei 11529, Taiwan, Republic of China*

⁴*Australian Nuclear Science and Technology Organisation, New Illawarra Rd, Lucas Heights, New South Wales 2234, Australia*

⁵*School of Chemistry, The University of Sydney, Sydney, New South Wales 2006, Australia*



(Received 2 September 2021; revised 28 September 2021; accepted 19 October 2021; published 28 October 2021)

We have investigated the magnetic structure of $\text{Li}_2\text{Co}(\text{WO}_4)_2$ via magnetic susceptibility, and neutron diffraction measurements. Two magnetic transitions are observed in magnetic susceptibility at $T_{N1} \sim 9.5$ K and $T_{N2} \sim 7.2$ K. Neutron diffraction reveals an incommensurate magnetic order with a wave vector $k_{\text{ICM}} = (\sim 0.46, \sim 0.27, \sim 0.24)$ between T_{N1} and T_{N2} and a commensurate magnetic order with a wave vector $k_{\text{CM}} = (0.5, 0.25, 0.25)$ below T_{N2} . The magnetic periodicity in the commensurate phase is four times larger than the nuclear unit cell length along the b - and c -axis directions with a saturated magnetic moment equal to $\approx 2.92 \mu_B$. Below T_{N1} , the ICM wave vector for $\text{Li}_2\text{Co}(\text{WO}_4)_2$ varies with decreasing temperature and locked into commensurate at T_{N2} , whereas weaker temperature dependence of $k_{\text{ICM}} = (0.46, 0.17, 0.33)$ is observed for $\text{Li}_2\text{Ni}(\text{WO}_4)_2$.

DOI: [10.1103/PhysRevB.104.134435](https://doi.org/10.1103/PhysRevB.104.134435)

I. INTRODUCTION

Low-dimensional and frustrated systems have attracted significant attention over the past years due to their highly interesting magnetic properties [1,2]. Frustration, i.e., the inability of a system to reach a single lowest energy state where all interactions are simultaneously satisfied, can have different origins in a magnetic system, e.g., particular lattice geometry, such as triangular or kagome, or competing magnetic interactions. In magnetism, frustration prevents the formation of magnetically ordered phases with the emergence of unusual phenomena such as spin liquids [2] and spin ice [3], which appear at low temperatures when a system fluctuates between different magnetic configurations. In other systems, an ordered frustrated state may emerge with the formation of commensurate/incommensurate magnetic structures. For instance, in quasi-one-dimensional (1D) compound LiCuVO_4 [4], the incommensurate magnetic ordering arises due to frustrated intrachain interactions, whereas in triangular lattice antiferromagnets such as CsNiCl_3 [5] and $\text{Li}_2\text{NiW}_2\text{O}_8$ [6], the magnetic ordering develops due to interchain magnetic interaction resulting from frustrated arrangement of chains. In a more recent work on 1D and two-dimensional (2D) Co spin systems, such as $\text{Pb}_3\text{TeCo}_3\text{V}_2\text{O}_{14}$ [7] and $\text{Ba}_3\text{CoNb}_2\text{O}_9$ [8], two-step successive magnetic phase transitions have been observed which are similar to the anomalies observed in $\text{Li}_2\text{Ni}(\text{WO}_4)_2$ [6,9] and $\text{Li}_2\text{Co}(\text{WO}_4)_2$ [10,11].

$\text{Li}_2M(\text{WO}_4)_2$ ($M = \text{Co}, \text{Ni}$) crystallizes into a triclinic structure having $P\bar{1}$ symmetry. The crystal structure can be viewed as a three-dimensional arrangement of isolated MO_6 octahedra that are corner shared with the double WO_4 group, which is deformed into an edge-shared inverted square pyramid WO_5 pair (inset of Fig. 2). The simplest view of $\text{Li}_2M(\text{WO}_4)_2$ is that the isolated MO_6 octahedra are bridged by a double WO_4 group, and the Li atoms sit in the interstitial site due to their ionic nature. Our previous works and similar report by Ranjit *et al.* on $\text{Li}_2\text{Ni}(\text{WO}_4)_2$ isostructural to $\text{Li}_2\text{Co}(\text{WO}_4)_2$ show two magnetic transitions ~ 13 and ~ 18 K corresponding to the commensurate to incommensurate and incommensurate to paramagnetic transitions, respectively [6,9,12]. Recently, the physical properties of the $\text{Li}_2\text{Co}(\text{WO}_4)_2$ [10,11] and $\text{Li}_2\text{CuW}_2\text{O}_8$ [13] have also been characterized in detail. Two magnetic phase transitions at 7.2 and 9.5 K have been observed in $\text{Li}_2\text{Co}(\text{WO}_4)_2$ but the magnetic structures of both phases are still unknown [10]. In this work we have solved the magnetic structures of both phases for $\text{Li}_2\text{Co}(\text{WO}_4)_2$ using neutron powder diffraction (NPD) and compared the results with isostructural $\text{Li}_2\text{Ni}(\text{WO}_4)_2$. Following the observation of the two magnetic anomalies revealed at $T_{N1} \sim 9.5$ K and $T_{N2} \sim 7.2$ K in the magnetic susceptibility $\chi(T)$ of $\text{Li}_2\text{Co}(\text{WO}_4)_2$, antiferromagnetic long-range spin ordering below $T_{N2} \sim 9.5$ K has been confirmed with neutron diffraction. A commensurate magnetic (CM) propagation vector $k_{\text{CM}} = (1/2, 1/4, 1/4)$ is determined below 7.2 K for $\text{Li}_2\text{Co}(\text{WO}_4)_2$, which is very different from $k = (1/2, 0, 1/2)$ observed below 13 K for $\text{Li}_2\text{Ni}(\text{WO}_4)_2$. Whereas incommensurate magnetic (ICM) reflections having $k_{\text{ICM}} = (0.46, 0.27, 0.24)$ are observed for $\text{Li}_2\text{Co}(\text{WO}_4)_2$ in the temperature range between $T_{N1} \sim 9.5$ K and $T_{N2} \sim 7.2$ K.

*skkarna@nsu.edu

†wang.cw@nsrrc.org.tw

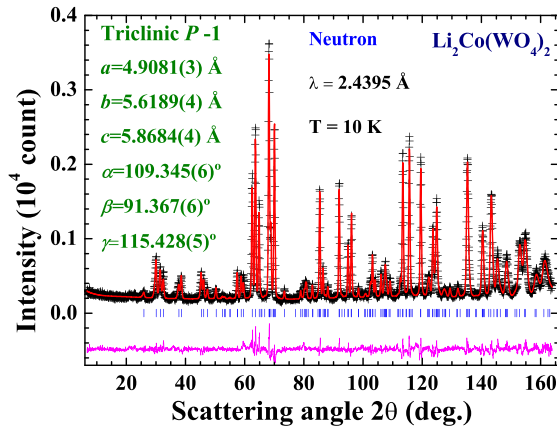


FIG. 1. Observed (crosses) and fitted (solid lines) neutron powder-diffraction patterns taken at 10 K, assuming a triclinic $P\bar{1}$ symmetry for the crystalline structure. The differences between the calculated and observed patterns are plotted at the bottom. The solid vertical lines mark the calculated positions of the Bragg reflections of the proposed crystalline structure presented in the inset of Fig. 2.

II. EXPERIMENTAL DETAILS

The polycrystalline samples of $\text{Li}_2(\text{Co, Ni})(\text{WO}_4)_2$ were synthesized using a solid-state method. Stoichiometric quantities of high purity ($>99.95\%$) powders of CoO , NiO , Li_2CO_3 , and WO_3 were mixed and heated at 550 and 650 °C for 24 h with intermittent grinding and pelletizing. Final annealing was performed at 700 °C for 160 h and followed by furnace cooling to room temperature at a rate of approximately 150 °C/h. The resultant compounds $\text{Li}_2\text{Co}(\text{WO}_4)_2$ and $\text{Li}_2\text{Ni}(\text{WO}_4)_2$ were purple and yellow, respectively. To check the phase purity of samples, x-ray diffraction measurements were performed on a Bruker D8 ADVANCE diffractometer employing $\text{Cu } K_\alpha$ radiation. X-ray and neutron powder diffraction measurements were used to determine the crystal structure of the sample. The neutron diffraction data were collected at Australia Nuclear Science and Technology Organisation (ANSTO) using the high-resolution powder diffractometer ECHIDNA [$\lambda = 2.4395 \text{ \AA}$ defined by Ge (331) crystals] for the crystal structure analysis, and the high-intensity powder diffractometer WOMBAT [$\lambda = 2.41 \text{ \AA}$ defined by Ge (115) crystals with 120° take-off angle, and $\lambda = 4.77 \text{ \AA}$ from PG (002) crystals with 90° take-off angle] for the magnetic structure analysis [14,15]. To achieve a good signal-to-noise ratio, each diffraction pattern was collected on ECHIDNA for 4 h with an angular step of 0.05° using approximately 4 g of sample loaded in a cylindrical vanadium can 6 mm in diameter. The sample temperature was controlled using a He-gas closed-cycle refrigeration system. The Rietveld refinement of NPD patterns were performed using the FullProf Suite [16]. The Thompson-Cox-Hasting pseudo-Voigt function and Chebychev polynomials were used for modeling the peak shape and background of the NPD patterns, respectively. Magnetic propagation vectors were obtained using the k -search program of FullProf Suite. The nuclear refinement of the neutron diffraction pattern of $\text{Li}_2\text{Co}(\text{WO}_4)_2$ at 10 K was performed assuming triclinic symmetry with a space group of $P\bar{1}$ (Fig. 1). No identifiable traces of impurity phases were present in the neutron diffraction patterns. The magnetic

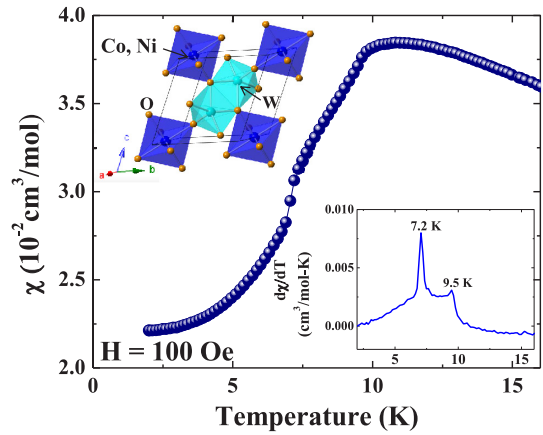


FIG. 2. Temperature dependence of magnetic susceptibilities for $\text{Li}_2\text{Co}(\text{WO}_4)_2$ measured at an applied field of $H_a = 100 \text{ Oe}$. Inset shows the crystal structure and $d\chi/dT$ vs T .

measurements were performed using the commercial vibrating sample magnetometer (VSM, Quantum Design, USA).

III. RESULTS AND DISCUSSION

The temperature T dependence of the magnetic susceptibility measured at $H = 100 \text{ Oe}$ indicates two step drops near ~ 9.5 and $\sim 7.2 \text{ K}$ (Fig. 2), as also clearly identified in $d\chi/dT$ (inset of Fig. 2) where the peaks appear at the corresponding temperatures. A fit of the modified Curie-Weiss (CW) law to the data above 140 K (not shown) yields an effective moment of $\mu_{\text{eff}} = 3.79 \mu_B/\text{Co}$ in agreement with the expected high spin value of Co^{2+} and $\theta_{\text{CW}} = -27 \text{ K}$, suggesting the antiferromagnetic nature of the spin interaction. The spin-only values of effective moment for Co^{2+} in high spin (HS, $t_{2g}^5 e_g^2$, $S = 3/2$) and low spin (LS, $t_{2g}^6 e_g^1$, $S = 1/2$) states are 3.872 and $1.73 \mu_B$, respectively. For Co^{2+} (LS), three t_{2g} orbitals, d_{xy} , d_{yz} , and d_{zx} , are all fully occupied, and no orbital angular momentum contribution to the magnetic moment is allowed in the ground state. Therefore, Co^{2+} in $\text{Li}_2\text{Co}(\text{WO}_4)_2$ is in the HS state with considerable orbital angular momentum contribution.

In order to clarify the nature of two phase transitions of $\text{Li}_2\text{Co}(\text{WO}_4)_2$, we performed neutron powder diffraction at different temperatures between 5 and 12 K. The NPD patterns collected above T_{N1} contain nuclear diffraction peaks only and can be used as the reference for identifying the magnetic signal. The nuclear contribution of the neutron diffraction pattern collected below 12 K has been subtracted to isolate the magnetic signal and plotted the differences as contour plot in Fig. 3(a) showing only the magnetic diffraction peaks (Fig. 4). Several magnetic diffraction peaks developed below T_{N1} move with the decreasing temperature. The magnetic propagation vector at each temperature is determined with the help of a k -search program of the FullProf Suite. Generally speaking, it is more difficult to determine incommensurate propagation vector for the parent structure having a low symmetry than that of a higher symmetry, especially when the number of available magnetic diffraction peaks is limited. We have determined the propagation vector for the CM phase first which

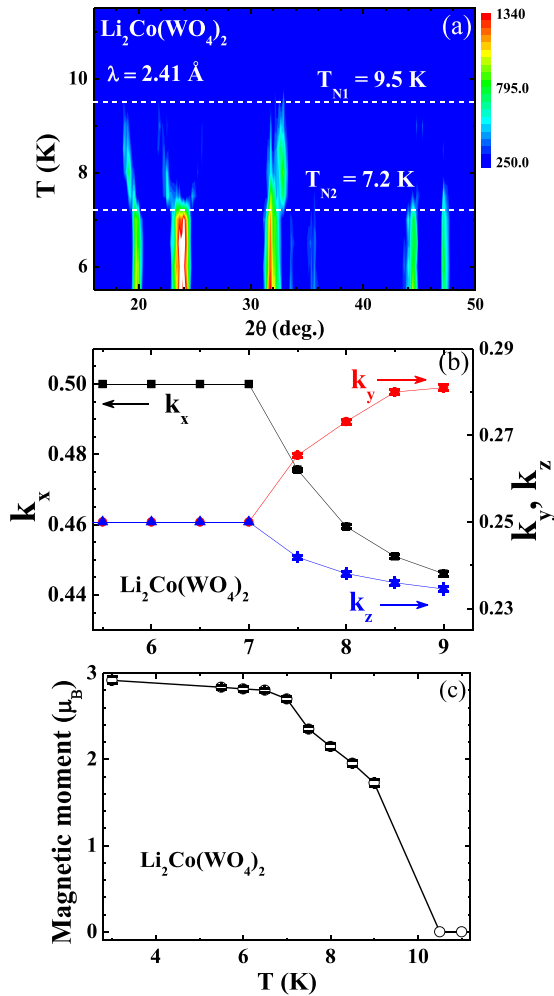


FIG. 3. (a) Contour plot showing the magnetic signals below T_{N1} as a function of temperature and scattering angle. Temperature dependence of (b) the components of incommensurate modulation k_x (left) and k_y , k_z (right), and (c) the refined magnetic moments.

is $\mathbf{k}_{\text{CM}} = (0.5, 0.25, 0.25)$, providing a reference values of k_x , k_y , and k_z for ICM. The three-component incommensurate modulation is characterized by a wave vector $\mathbf{k}_{\text{ICM}} = (k_x, k_y, k_z)$ where k_x , k_y , and k_z are ~ 0.44 , ~ 0.3 , and ~ 0.23 respectively. All three components shift monotonically with the decreasing temperature, and lock-in to $(0.5, 0.25, 0.25)$ at T_{N2} . One can observe that diffraction peaks move with decreasing temperature between T_{N1} and T_{N2} , whereas below T_{N2} the peak positions exhibit independent of temperature implying that $\text{Li}_2\text{Co}(\text{WO}_4)_2$ at first enters into an incommensurate magnetic phase with a temperature dependent propagation vector \mathbf{k} , followed by a lock-in transition into a commensurate phase.

Figure 3(b) shows the temperature dependence of the wave vectors for CM and ICM phases. The CM wave vector $\mathbf{k}_{\text{CM}} = (0.5, 0.25, 0.25)$ involving magnetic periodicity quadruples the direct unit cell length along the b - and c -axis directions. Such type of magnetic periodicity is not rare but has also been observed in several systems. For example, MnWO_4 , RMn_2O_5 ($R = \text{Y, Ho, Tb, Er}$), $\text{Tm}_3\text{Cu}_4\text{Ge}_4$, and $\text{Tm}_3\text{Cu}_4\text{Sn}_4$

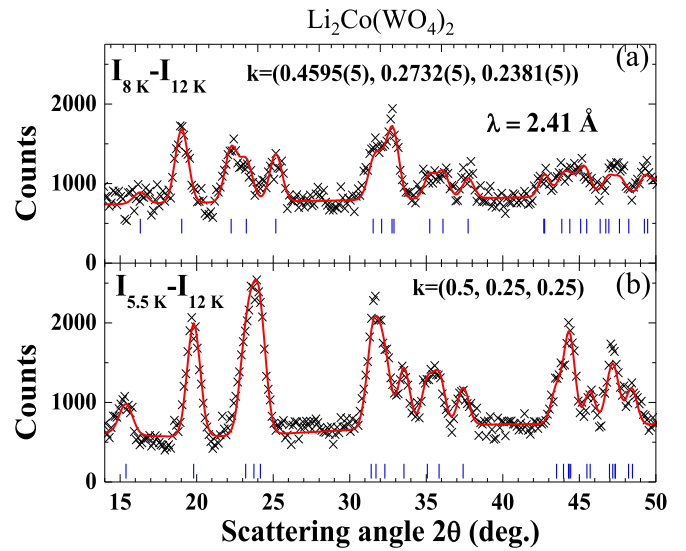


FIG. 4. Magnetic diffraction pattern obtained at (a) 8 K (ICM phase) and (b) 5.5 K (CM phase), where the solid curves are the Rietveld fit to the data, yielding the magnetic structures presented in Fig. 6. The solid vertical lines mark the calculated positions of the magnetic Bragg reflections of the proposed magnetic structure.

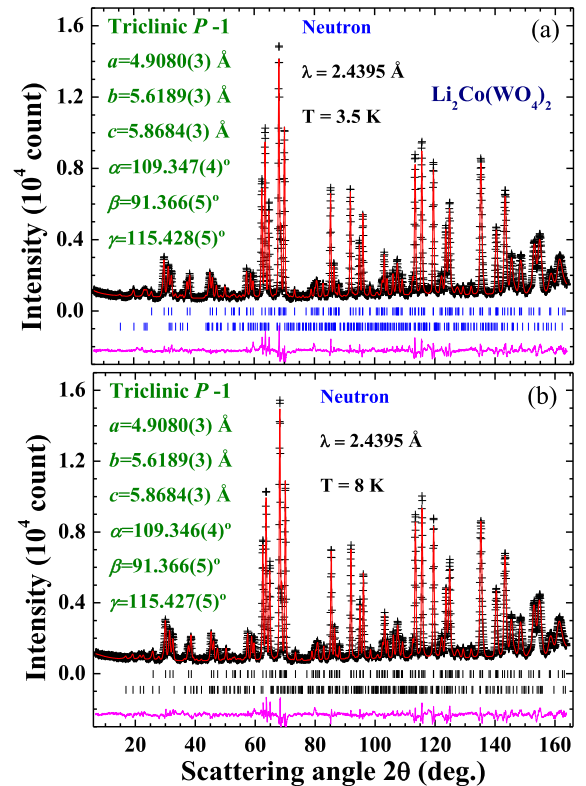


FIG. 5. Observed (crosses) and fitted (solid lines) neutron powder-diffraction patterns taken at (a) 3.55 K and (b) 8 K assuming a triclinic $P\bar{1}$ symmetry for both the crystalline and magnetic structures. The differences between the calculated and observed patterns are plotted at the bottom. The two sets of solid vertical lines mark the calculated positions of the Bragg reflections of the proposed crystalline and magnetic structures.

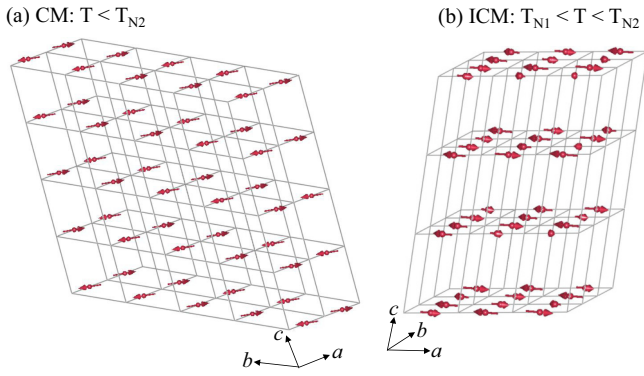


FIG. 6. A schematic antiferromagnetic spin structure of $\text{Li}_2\text{Co}(\text{WO}_4)_2$: (a) CM phase below T_{N2} , and (b) ICM phase between T_{N1} and T_{N2} based on the fitting of neutron diffraction data.

possess a quarter wave vector along one or more reciprocal lattice directions in both CM and ICM phases [17–21]. Due to the special case of the propagation vector being a quarter of the reciprocal lattice vector, i.e., $k_y = k_z = 0.25$, the magnetic structure contains paramagnetic moments of zero static moment. When we view the spin structure along the b and c directions, the magnetic moments of Co^{2+} ions are in sequence of $\dots m, 0, -m, 0, \dots$, where $m = 4.125 \mu_B$. Alternately, we can exclude the paramagnetic moments by introducing a phase factor of $\pi/4$, leaving the calculated magnetic diffraction peak intensities unchanged. In the new

model, all the magnetic moments are of equal magnitude and the sequence along the b and c directions now become $\dots m', m', -m', -m', \dots$, where $m' = 2.917 \mu_B$. We do not observe any structure modulation with the same k vector so that the local environment for all the Co^{2+} ions are identical. Therefore, the Co should not possess different values of magnetic moment. The Rietveld refinement of the NPD patterns at 3.5 and 8 K are presented in Fig. 5 and the corresponding magnetic structures for both CM and ICM phases are shown in Fig. 6.

The temperature dependence of magnetic moments obtained from the refinement is displayed in Fig. 3(c). The expected spin only value of the static moment $\langle \mu_z \rangle = gS$ for Co^{2+} in LS and HS state are 1 and $3 \mu_B$, respectively. The high spin state is favored which is consistent with the effective moment $\langle \mu_{\text{eff}} \rangle$ in the paramagnetic phase. However, the observed static magnetic moments in both models are smaller than the moment of $\text{Co}^{2+}(\text{HS})$ with the full contribution of orbital angular momentum which is $\langle \mu_z \rangle = g_J J = 6 \mu_B$. We suggest that the missing magnetic moment might be due to the quenched orbital contribution below T_N , which is common for Co^{2+} [22]. In general, the $\dots m', m', -m', -m', \dots$ spin arrangement might occur when there is geometric spin frustration with the frustration index value of $|\frac{6_{\text{CW}}}{T_N}| \sim 2.8$ for $\text{Li}_2\text{Co}(\text{WO}_4)_2$ does suggest mild frustration.

Another isostructural analog $\text{Li}_2\text{Ni}(\text{WO}_4)_2$ undergoes magnetic phase transitions at $T_{N1} \sim 18$ K and $T_{N2} \sim 13$ K [9,12]. The Curie-Weiss fit to the high temperature part of

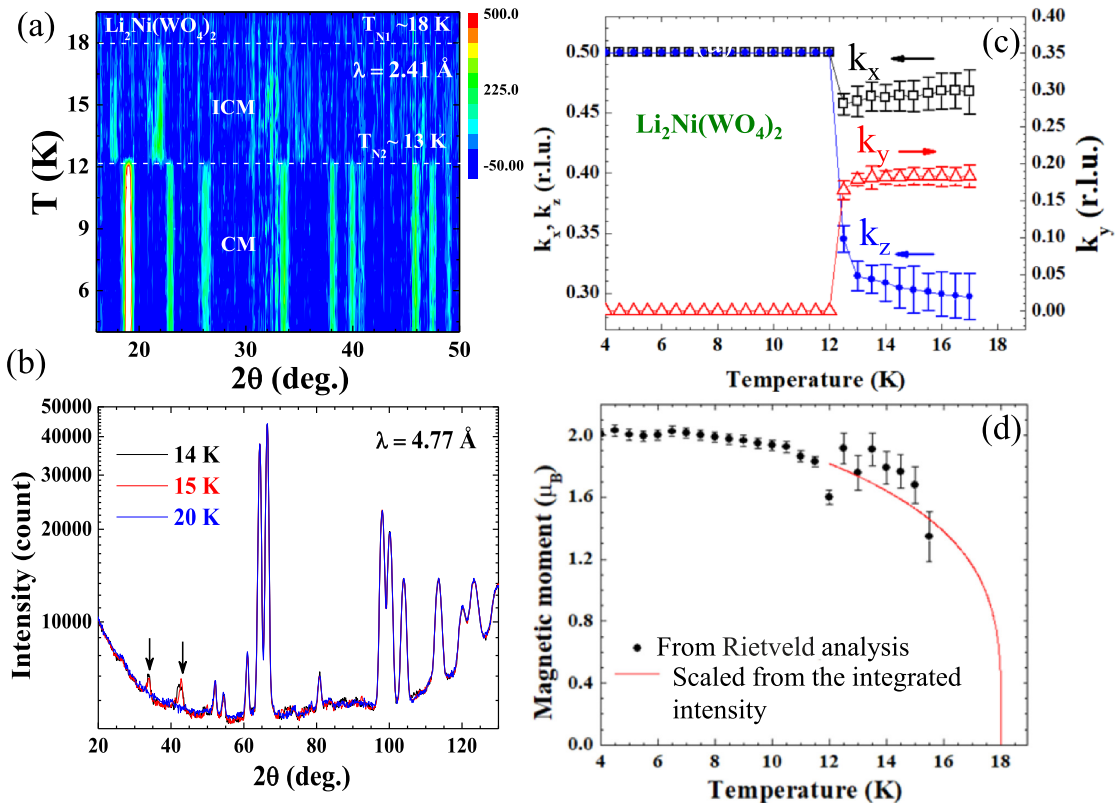


FIG. 7. (a) Contour plot showing the magnetic signals below T_{N1} for $\text{Li}_2\text{Ni}(\text{WO}_4)_2$ as a function of temperature and scattering angle. (b) NPD patterns at the indicated temperatures. (c) The components of incommensurate modulation k_x , k_z (left), and k_y (right). (d) Temperature dependence of the refined magnetic moments.

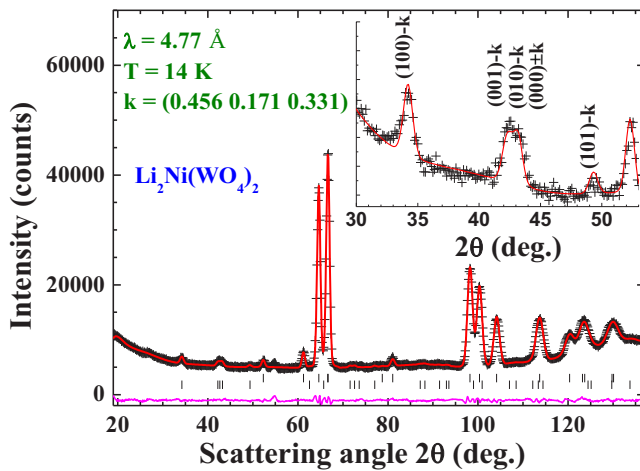


FIG. 8. Rietveld refinement of neutron powder-diffraction patterns at 14 K, assuming a triclinic $P\bar{1}$ symmetry for both the crystalline and magnetic structures. The differences between the calculated and observed patterns are plotted at the bottom. The two sets of solid vertical lines mark the calculated positions of the Bragg reflections of the proposed crystalline and magnetic structures. The inset shows the amplified view of the ICM peak that appears below $T_{N1} \sim 18$ K.

$\chi(T)$ gives the $\mu_{\text{eff}} = 3.06 \mu_B/\text{Ni}$ is slightly larger (not significantly) with a minor orbital contribution in accord with the expected spin only value $2.83 \mu_B$, as discussed in Refs. [10–12]. Both compounds exhibit very similar features in magnetic susceptibility except the upturn observed ~ 9 K in $\text{Li}_2\text{Ni}(\text{WO}_4)_2$ which might be explained by Curie tail from impurity and/or lattice imperfections in the sample [9,12].

We have also collected powder neutron diffraction patterns on $\text{Li}_2\text{Ni}(\text{WO}_4)_2$ at several temperatures below 20 K. Because the observed magnetic reflections are considerably weaker than nuclear structure diffraction peaks, we have subtracted the diffraction patterns of 19.5 K collected well above T_{N1} from the diffraction patterns at different temperatures below T_{N1} and displayed the magnetic scattering as a contour plot in Fig. 7(a). One can see two very distinct magnetic phases appear above and below T_{N2} . Surprisingly, they are very different than the magnetic phases of $\text{Li}_2\text{Co}(\text{WO}_4)_2$ which may be due to the absolute values of the exchange interaction parameters

for $\text{Li}_2\text{Ni}(\text{WO}_4)_2$ obtained from *ab initio* calculations which are ~ 2 times larger than that for $\text{Li}_2\text{Co}(\text{WO}_4)_2$ [9,10,12]. For $\text{Li}_2\text{Ni}(\text{WO}_4)_2$, the magnetic peak positions of the ICM magnetic phase between T_{N1} and T_{N2} are not as sensitive to the temperature as in $\text{Li}_2\text{Co}(\text{WO}_4)_2$ where temperature dependent ICM phase is observed. Figure 7(c) shows the temperature dependence of the ICM and CM wave vectors for $\text{Li}_2\text{Ni}(\text{WO}_4)_2$. It can be seen that the CM wave vector \mathbf{k}_{CM} is (0.5, 0, 0.5) below T_{N2} in agreement with previous reports [6,9], whereas ICM wave vector obtained at 14 K between T_{N1} and T_{N2} is (0.456, 0.171, 0.331). The Rietveld refinement of the NPD patterns of ICM phase at 14 K is displayed in Fig. 8. The magnetic moments obtained from the refinement is displayed in Fig. 7(d). Due to weaker magnetic signals above 15 K, the magnetic moments are estimated and scaled from the integrated intensity and presented by a solid red line in Fig. 7(d).

IV. CONCLUSIONS

In summary, we have conducted detailed magnetic neutron diffraction studies of $\text{Li}_2\text{Co}(\text{WO}_4)_2$ and compared the results with isostructural analog $\text{Li}_2\text{Ni}(\text{WO}_4)_2$. The incommensurate phase evolves with decreasing temperature below T_{N1} and locks into commensurate magnetic structure at T_{N2} for both compounds. A much larger CM magnetic unit cell is realized for $\text{Li}_2\text{Co}(\text{WO}_4)_2$ with the Co spins in (+ + - -) sequence when moving to the neighboring magnetic sites along b and c axis. The different magnetic ground states of the two isostructural compounds indicate the differences in the magnetic couplings.

ACKNOWLEDGMENTS

S.K.K acknowledges the support from the National Science Foundation through Excellence in Research: Single Crystal Growth and Investigation of Novel Exotic Fermion Materials program under award DMR-1832031. C.W.W. acknowledges the travel support provided by National Synchrotron Radiation Research Center (NSRRC). R.S. acknowledges financial support provided by the Ministry of Science and Technology in Taiwan under Projects No. MOST-110-2112-M-001-065-MY3 and No. MOST 109-2124-M-002-001. We thank ANSTO for providing the neutron beam time that made the neutron diffraction measurements possible.

- [1] A. Ramirez, *Annu. Rev. Mater. Sci.* **24**, 453 (1994).
- [2] L. Balents, *Nature (London)* **464**, 199 (2010).
- [3] S. T. Bramwell and M. J. Gingras, *Science* **294**, 1495 (2001).
- [4] M. Mourgil, M. Enderle, R. K. Kremer, J. M. Law, and B. Fåk, *Phys. Rev. B* **83**, 100409(R) (2011)
- [5] R. M. Morra, W. J. L. Buyers, R. L. Armstrong, and K. Hirakawa, *Phys. Rev. B* **38**, 543 (1988).
- [6] K. M. Ranjith, R. Nath, M. Majumder, D. Kasinathan, M. Skoulatos, L. Keller, Y. Skourski, M. Baenitz, and A. A. Tsirlin, *Phys. Rev. B* **94**, 014415 (2016).
- [7] M. M. Markina, B. V. Mill, E. A. Zvereva, A. V. Ushakov, S. V. Streltsov, and A. N. Vasiliev, *Phys. Rev. B* **89**, 104409 (2014).
- [8] K. Yokota, N. Kurita, and H. Tanaka, *Phys. Rev. B* **90**, 014403 (2014).
- [9] S. K. Karna, C. W. Wang, R. Sankar, M. Avdeev, A. Singh, I. Panneer Muthuselvam, V. N. Singh, G. Y. Guo, and F. C. Chou, *Phys. Rev. B* **92**, 014413 (2015).
- [10] I. P. Muthuselvam, R. Sankar, A. V. Ushakov, G. N. Rao, S. V. Streltsov and F. C. Chou, *Phys. Rev. B* **90**, 174430 (2014).
- [11] C.-W. Wang, S. Karna, F. C. Chou and R. Sankar, in *40th Annual Condensed Matter and Materials Meeting* (Australian Institute of Physics, Wagga, NSW, 2016).
- [12] I. Panneer Muthuselvam R. Sankar, A. V. Ushakov, W. T. Chen, G. Narsinga Rao, S. V. Streltsov, S. K. Karna, L. Zhao, M. K.

- Wu, and F. C. Chou, *J. Phys.: Condens. Matter* **27**, 456001 (2015).
- [13] K. M. Ranjith, R. Nath, M. Skoulatos, L. Keller, D. Kasinathan, Y. Skourski, and A. A. Tsirlin, *Phys. Rev. B* **92**, 094426 (2015).
- [14] M. Avdeev and J. R. Hester, *J. Appl. Crystallogr.* **51**, 1597 (2018).
- [15] A. J. Studer, M. E. Hagen, and T. J. Noakes, *Phys. B: Condens. Matter* **385-386**, 1013 (2006).
- [16] J. Rodriguez-Carvajal, *Physica B (Amsterdam)* **192**, 55 (1993).
- [17] G. Lautenschlager, H. Weitzel, T. Vogt, R. Hock, A. Bohm, M. Bonnet, and H. Fuess, *Phys. Rev. B* **48**, 6087 (1993).
- [18] C. Vecchini, L. C. Chapon, P. J. Brown, T. Chatterji, S. Park, S.-W. Cheong, and P. G. Radaelli, *Phys. Rev. B* **77**, 134434 (2008).
- [19] S. Kobayashi, T. Osawa, H. Kimura, Y. Noda, N. Kasahara, S. Mitsuda, and K. Kohn, *J. Phys. Soc. Jpn.* **73**, 3439 (2004).
- [20] S. Kobayashi, T. Osawa, H. Kimura, Y. Noda, I. Kagomiya, and K. Kohn, *J. Phys. Soc. Jpn.* **73**, 1031 (2004).
- [21] S. Baran, D. Kaczorowski, A. Szytuła, A. Gil, and A. Hoser, *J. Phys.: Condens. Matter* **25**, 066012 (2013).
- [22] L. Ortega-San Martin, J. P. Chapman, L. Lezama, J. Sánchez-Marcos, J. Rodríguez-Fernández, M. I. Arriortua and T. Rojo, *J. Mater. Chem.* **15**, 183 (2005).